# Digital Refining Equivalent Model of Winding Bars of Turbogenerator Stator End

Ye Fan, Ting Wang* and Meishu Xiong

*Abstract*—**Given the complex structure of the wire rod of the stator end winding of a large turbine generator, this paper studies the equivalent method of the wire rod. We performed a three-point bending test on the wire rod structure using finite element software to obtain the bending stiffness and deflection of the wire rod. Then, the equivalent wire rod was established by a reasonable method. Moreover, the simplified wire rod is used to build the structure of turbogenerator end winding to reduce the calculation time. A mathematical model of the vibration of the stator end winding is developed by equating it to a composite shell to reflect its vibration characteristics. These research results will assist in designing and improving generator end structures.**

*Index Terms*—**steam turbine generator; finite element; ansys; equivalent model**

## I. Introduction

THE stator winding is a crucial component of the turbogenerator and is pivotal in converting mechanical energy into electrical energy. The end extension of the generator stator winding exhibits a highly complex, non-linear and strongly spatially curved geometry. Given the intricate nature of the geometry and the material properties, it is significant to establish a reasonable 3D model of the stator end winding and to determine the material properties [1]-[2].

Generally, the stator winding of a large turbogenerator adopts a stacked winding. The end of the stator winding protrudes from the stator core and then slopes outward. Because stator winding is formed by bending and weaving on the conical surface along a cone angle of 30º or less double-layer basket structure, it is also called basket winding. As the generator capacity and voltage level continue to increase, the temperature rise generated by the stator winding, the main heat-generating component of the generator, also increases accordingly. Accidents caused by overheating stator windings occur constantly, so efficient cooling measures such as reducing the heat generated by the stator winding can ensure the safe operation of the generator [3]-[5]. Most large turbogenerator end winding structures in China use water cooling for cooling.

In addition, many solid and hollow flat copper wires are tightly woven on the stator wire rod, allowing the cooling water to flow through the hollow wires. The heat generated by the windings can be dissipated by the water flow, thus preventing accidents caused by winding insulation wear due to high temperatures. The ends of the upper and lower wire rods are evenly distributed along the cone surface, and their cross-sectional structure is shown in Fig. 1 [6].

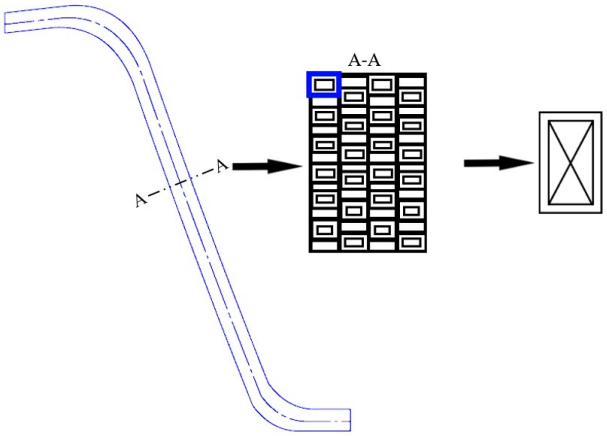


Fig. 1. Unfolded and cross-section drawing of bars.

The present study aims to investigate the vibration behavior of the equivalent structure of stator winding. The subsequent sections are organized as follows. In the next section, we establish the equivalent structure of the winding based on the theory of bending stiffness. In the third section, a mathematical model is developed to predict the vibration behavior of the equivalent structure. The results from this model are compared with finite element analysis to validate the model's accuracy. Moreover, we investigate the effect of the wire rod's material properties on the structure's intrinsic frequency. Finally, the fourth section summarises the findings.

## II. Equivalent of Wire Rod

### A. Necessity of equivalence

All the details of the wire rod are considered to establish a finite element model. Due to the hollow structure and the insulating layer, each wire rod needs to be divided into a large number of cells. A large number of meshes can lead to an increase in computational effort. Therefore, it is necessary to

Manuscript received May 19, 2022; revised April 29, 2023.

The work was supported by National Natural Science Foundation of China (Grant No.51807019), the Science and Technology Research Program of Chongqing Municipal Education Commission (KJZD-K201900604), the Open Projects of State Key Laboratory for Strength and Vibration of Mechanical Structures (Grant No. SV2020-KF-15), Chongqing Special Postdoctoral Science Foundation (Grant No.XmT2018030) .

Y. Fan is a postgraduate student of School of Chongqing University of Posts and Telecommunications (CQUPT), Chongqing 400065, China (e-mail: S212101002@stu.cqupt.edu.cn).

T. Wang is a professor in the Key Laboratory of Industrial Internet of Things and Networked Control, Ministry of education, Chongqing University of Posts and Telecommunications (CQUPT), Chongqing 400065, China (e-mail: wangting@cqupt.edu.cn).

M. S. Xiong is an associate professor of School of Chongqing University of Posts and Telecommunications (CQUPT), Chongqing 400065, China (e-mail: xiongms@cqupt.edu.cn).

carry out an equivalent to reduce the calculation scale.

### B. Equivalence principle of wire rod

Based on the above reasons, a solid equivalent wire bar can be used instead of the actual wire bar. Whether the elliptical mode is of interest or the deformation under electromagnetic force during the running, the wire bar mainly shows bending deformation. When equating the wire rod, the bending stiffness in the height and width directions should be equal, in addition to the requirement that the mass of the equated model is equivalent to that of the model before equating. The equivalent mass of the equivalent bar and the actual bar can be achieved by modifying its density.

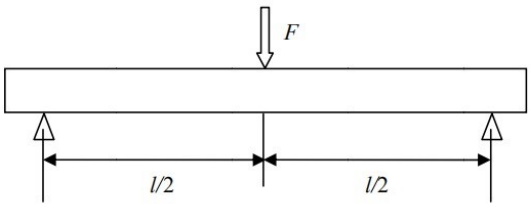


Fig. 2. Three-point bending test.

The three-point bending test is shown in Fig. 2, where the formula for calculating the deflection of the midpoint at the bar is:

$$f_{\max} = \frac{Fl^3}{48EI} \quad (1)$$

The formula of the bending stiffness of the wire rod is:

$$EI = \frac{l^3}{48}\left(\frac{\Delta F}{\Delta l}\right) \quad (2)$$

The formula for the conservation of mass is:

$$\rho_1 V_1 = \rho_2 V_2 \quad (3)$$

### C. Equivalent model of wire rod

The finite element method was used to simulate the three-point bending test of the straight section of the bar before the equivalent, and its deflection and bending stiffness were obtained. A hollow rectangular section bar model is established. The finite element model and the calculated deflection curve are shown in Fig. 3. The calculated deflection is given in Table I.

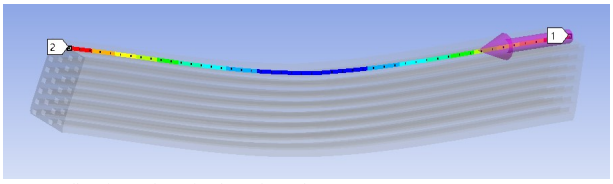

Fig 3. Deflection of equivalent front bar.

TABLE I
TNUMERICAL SIMULATION OF THREE-POINT BENDING DEFLECTION OF EQUIVALENT FRONT BAR

| Direction | Deflection(mm) | |
|---|---|---|
| | Load 5000N | Load 8000N |
| height | 0.269 | 0.428 |
| width | 0.521 | 0.834 |

To make the bending stiffness of the equivalent bar constant, that is:

$$EI_x = E\frac{ab^3}{12} = 5.128\times10^{10}\, Mpa\cdot mm^4 \quad (4)$$

$$EI_y = E\frac{ba^3}{12} = 2.346\times10^{10}\, MPa\cdot mm^4 \quad (5)$$

There are three unknown quantities in the above two equations. First, the equivalent cross-sectional dimensions a and b are the same as the actual dimensions. Then the value of the equivalent elastic modulus $E$ can be obtained. This equal efficiency guarantees that its stiffness is the same as that of the equivalent front bar.

The finite element was used to simulate the three-point bending test of the equivalent straight section of wire rod, and a solid rectangular section wire rod model was established. The finite element model and the calculated deflection curve are shown in Fig. 4. The deflections obtained from the equivalent front and rear wire rods are given in Table II.

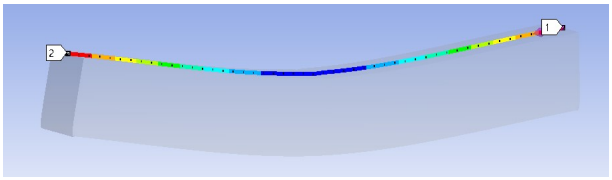

Fig 4. Deflection of the equivalent rear bar.

TABLE II
COMPARISON OF NUMERICAL SIMULATION OF THREE-POINT BENDING DEFLECTION OF EQUIVALENT FRONT BAR AND EQUIVALENT BACK BAR

| Direction | Deflection(mm) | | | |
|---|---|---|---|---|
| | Load 5000N | | Load 8000N | |
| | Before equivalent | After equivalent | Before equivalent | After equivalent |
| height | 0.269 | 0.267 | 0.428 | 0.427 |
| width | 0.521 | 0.515 | 0.834 | 0.828 |

## III. DIGITAL EQUIVALENT MODEL OF THE END WINDING

### A. Modal analysis of a single wire rod

In this study, the aim is to analyze the dynamic characteristics of the stator end windings of a turbogenerator. Modal analysis of the stator bar is conducted as a preliminary step to obtain the inherent vibration properties of the single bar.

The modeling of the stator end winding bar is performed based on the method described in [7]. The validity of this equivalent method is verified by performing a modal analysis on the equivalent front and rear wire bars. Modal parameters such as modal frequencies and modal shapes are compared before and after equivalence. It is noted that the stator winding is embedded in the inner circle of the stator core, and all nodes of the straight section of the winding have full displacement constraints. The modal analysis is presented in Fig. 5. It can be seen that the natural frequency and mode errors of the equivalent front and rear bars are minor, indicating the accuracy of the equivalent method.

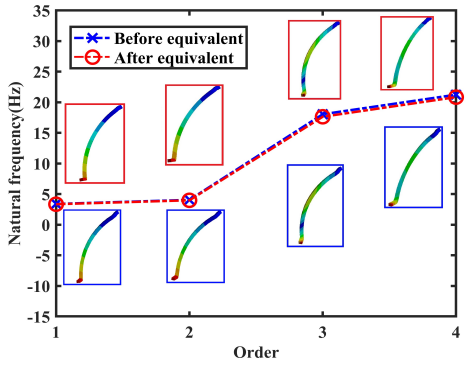


Fig 5. Comparison of modal parameters equivalence of wire rod.

### *B. The establishment of the vibration model*

This study aims to develop a mathematical model of the stator end winding structure and evaluate its accuracy. The effectiveness of the equivalent wire rod is verified by modal analysis, and then this structure is applied to the numerical refinement model. For mathematical modeling, this structure is used to reduce the modeling difficulty; for finite element modeling, this structure is used to improve computational efficiency.

A mathematical model is deemed valuable to reflect the vibration characteristics of the stator end winding structure. However, the actual structure is complex, and a simplified approach is adopted to reduce the modeling difficulty, as described in [8]. The test results indicate that the vibration characteristics of the structure of stator end winding reflect good integrity and are similar to those of a complete continuous medium, providing a reliable basis for developing an approximate theoretical calculation model [9].

The specific simplification and equivalence methods are described as follows. The lamellar tandem model in composite theory is used in the first step [10]. The equivalent wire rods are considered fibers, and the interlamellar rings are considered a matrix. Based on this assumption, a single-layer winding can be equivalent to a unidirectional fiber-reinforced material structure. Both upper and lower winding structures are so equated. A two-layer, truncated conical shell model is finally obtained by assuming that the upper and lower composite layers are closely fitted. The equivalent structure is shown in Fig. 6. The characteristic equation of the vibration of this equivalent shell is established based on the Rayleigh-Ritz method [11]-[13].

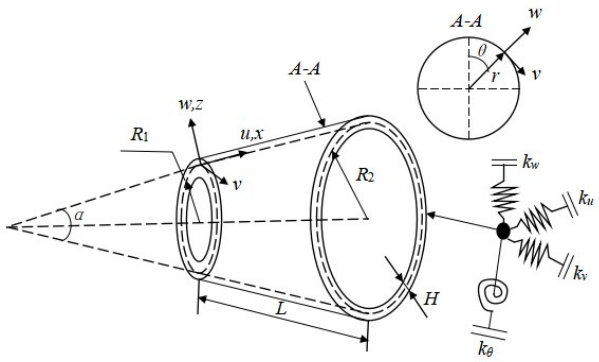


Fig 6. Equivalent shell structure schematic.

Establish an orthogonal curve coordinate system($x$,$\theta$,$z$) at the intersection of composite layers. The $x$-coordinate is the direction along the bus of the cone shell surface; the $z$-coordinate is the direction along the vertical cone shell surface; and the $\theta$-coordinate is the direction tangential to the radius of the cone shell. $R_1$ is the radius of the small diameter end; $R_2$ is the radius of the large diameter end; alpha is the number of half cone angles; $L$ is the length of the bus bar; and $H$ is the thickness of the shell. The boundary conditions are simulated by uniformly distributed artificial springs at the two end faces of the conical shell. $k_u$, $k_v$, $k_w$, and $k_\theta$ are the stiffnesses of the axial, circumferential, radial, and coiled springs, respectively.

Based on the Reissner shell theory [13], the geometric equations of strain, curvature, and torsion at the intersection are divided as follows:

$$\begin{aligned}
&\varepsilon_x^0=\frac{\partial u}{\partial x},\varepsilon_\theta^0=\frac{1}{R(x)}\frac{\partial v}{\partial \theta}+\frac{u\sin\alpha+w\cos\alpha}{R(x)}\\
&\gamma_{x\theta}^0=\frac{1}{R(x)}\frac{\partial u}{\partial \theta}+\frac{\partial v}{\partial x}-\frac{v\sin\alpha}{R(x)},k_x^0=-\frac{\partial^2 w}{\partial x^2}\\
&k_\theta^0=-\frac{1}{R^2(x)}\frac{\partial^2 w}{\partial \theta^2}+\frac{\cos\alpha}{R^2(x)}\frac{\partial v}{\partial \theta}-\frac{\sin\alpha}{R(x)}\frac{\partial w}{\partial x}\\
&\tau_{x\theta}^0=2\left(-\frac{1}{R(x)}\frac{\partial^2 w}{\partial x\partial \theta}+\frac{\sin\alpha}{R^2(x)}\frac{\partial w}{\partial \theta}\right)+\\
&2\left(\frac{\cos\alpha}{R(x)}\frac{\partial v}{\partial x}-\frac{v\sin\alpha\cos\alpha}{R^2(x)}\right)
\end{aligned}\tag{6}$$

where the radius function of the circular cross-section is $R(x)=R_1+x\sin\alpha$.

The vibration displacements $u$, $v$, and $w$ are expressed as the product of the circumferential displacement function and the axial mode [14]. The axial modes are expanded using a modified Fourier series [15], then

$$\begin{cases}
u=\left(\sum_{m=0}^{M}A_m\cos\frac{m\pi}{L}x+\sum_{l=1}^{2}a_l\zeta_l(x)\right)\cos(n\theta+\omega t)\\
v=\left(\sum_{m=0}^{M}B_m\cos\frac{m\pi}{L}x+\sum_{l=1}^{2}b_l\zeta_l(x)\right)\sin(n\theta+\omega t)\\
w=\left(\sum_{m=0}^{M}C_m\cos\frac{m\pi}{L}x+\sum_{l=1}^{4}c_l\zeta_l(x)\right)\cos(n\theta+\omega t)
\end{cases}\tag{7}$$

where $M$ is the number of truncation levels, and $\zeta_1(x)$, $\zeta_2(x)$, $\zeta_3(x)$, and $\zeta_4(x)$ are the auxiliary functions. Theoretically, these auxiliary functions can be chosen in any desired form. The selection rules only need to satisfy the existence of first-order differentiation of $u$ and $v$, the existence of third-order differentiation of $w$, and the continuity of any point on the cone shell.

The kinetic energy of the shell can be expressed as:

$$T=\frac{1}{2}\rho H\int_0^L\int_0^{2\pi}\left[\left(\frac{\partial u}{\partial t}\right)^2+\left(\frac{\partial v}{\partial t}\right)^2+\left(\frac{\partial w}{\partial t}\right)^2\right]R(x)d\theta dx\tag{8}$$

The strain energy of the shell can be expressed as:

$$V_\varepsilon=\frac{1}{2}\int_0^L\int_0^{2\pi}\varepsilon^{\mathrm{T}}\left[N_x\ N_\theta\ N_{x\theta}\ M_x\ M_\theta\ M_{x\theta}\right]^{\mathrm{T}}R(x)d\theta dx\tag{9}$$

where the strain vector and the internal force vector are expressed as follows:

$$\begin{cases}
\varepsilon^{\mathrm{T}}=\left[\varepsilon_x^0\quad\varepsilon_\theta^0\quad\gamma_{x\theta}^0\quad k_x^0\quad k_{x\theta}^0\quad\tau_{x\theta}^0\right]\\
\left[N_x\quad N_\theta\quad N_{x\theta}\quad M_x\quad M_\theta\quad M_{x\theta}\right]^{\mathrm{T}}=[S]\varepsilon
\end{cases}\tag{10}$$

where $[S]$ is the intrinsic relationship of the structure, which

is derived from the laminated composite of the lamellar tandem model in the theory of composite materials and is not repeated in this paper. Refer to [16] for the derivation process.

The potential energy of elastic boundary is as follows:

$$V_b = \frac{1}{2}\int_0^{2\pi}\left[k_{u0}u^2 + k_{v0}v^2 + k_{w0}w^2 + k_{\theta 0}\left(\frac{\partial w}{\partial x}\right)^2\right]_{x=0} R_1 d\theta + \frac{1}{2}\int_0^{2\pi}\left[k_{u1}u^2 + k_{v1}v^2 + k_{w1}w^2 + k_{\theta 1}\left(\frac{\partial w}{\partial x}\right)^2\right]_{x=L} R_2 d\theta \quad (11)$$

In summary, the Lagrangian function of the system is expressed as:

$$L = T - V_\varepsilon - V_b \quad (12)$$

Applying the Ritz method to derive the transformation yields the vibration characteristic equation of the structure as:

$$\left([\mathbf{K}] - \omega^2[\mathbf{M}]\right)\begin{Bmatrix}\overline{\mathbf{U}}\\ \overline{\mathbf{V}}\\ \overline{\mathbf{W}}\end{Bmatrix} = 0 \quad (13)$$

where $\overline{\mathbf{U}}=\{A_0,...,A_M,a_1,a_2\}^{\mathrm{T}}$, $\overline{\mathbf{V}}=\{B_0,...,B_M,b_1,b_2\}^{\mathrm{T}}$, and $\overline{\mathbf{W}}=\{C_0,...,C_M,c_1,c_2,c_3,c_4\}^{\mathrm{T}}$ are the vector coefficient. $[\mathbf{K}]$ and $[\mathbf{M}]$ are the stiffness matrix and the mass matrix respectively.

### C. *Numerical calculation and modal analysis*

The equivalent wire rod is used to build the finite element model of the end winding to improve computational efficiency. The stator end winding includes the ends of the upper and lower conductor bars and the spacer between adjacent conductor bars. Moreover, there are inter-layer rings between the upper and lower conductor bars. The 3D solid finally is shown in Fig. 7.

The wire rod uses the equivalent material, which density, elastic modulus, and Poisson's ratio are shown in Table III. The physical parameters of the structure, geometric parameters, and boundary conditions are brought into the mathematical model to solve the analytical solution. The modal parameters are obtained by modal analysis of the stator end windings using finite element analysis. The comparison of the two inherent frequencies is shown in Table IV, and the comparison of the corresponding vibration modes is shown in Figs. 8-11.

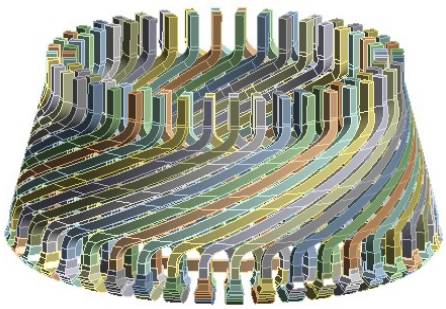

Fig7. Stator end windings model.

TABLE III
PHYSICAL AND MECHANICAL PROPERTIES OF STATOR END WINDINGS COMPONENTS

| Member | Young's modulus (Mpa) | Poisson's ratio | Density (kg/m$^3$) |
|---|---|---|---|
| Condutor bar | 38000 | 0.3 | 8800 |
| Space block | 23125 | 0.364 | 1798 |

TABLE IV
MODAL FREQUENCY DISTRIBUTION OF STATOR END WINDINGS

| Mode shape | Shake | Ellipse | Three-lobed | Four-lobed |
|---|---|---|---|---|
| Frequency/Hz (FEA) | 64.278 | 58.555 | 78.593 | 113.09 |
| | 64.295 | 58.582 | 78.727 | 113.35 |
| Frequency/Hz (Math Method) | 67.9486 | 63.5636 | 74.2289 | 106.0542 |

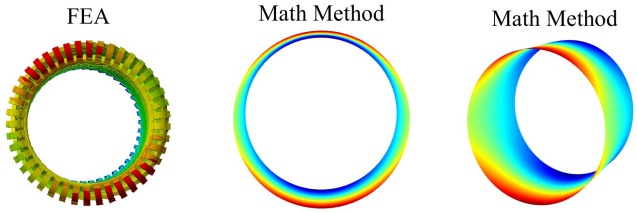


Fig8. Shake type.

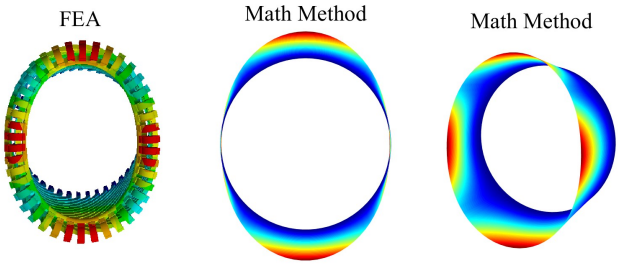


Fig9. Ellipse type.

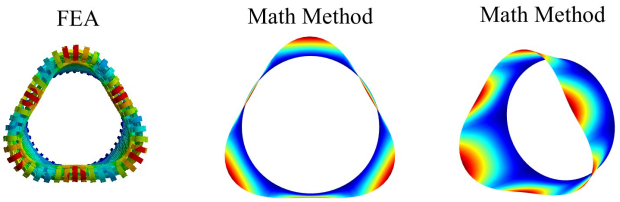


Fig10. Three-lobed.

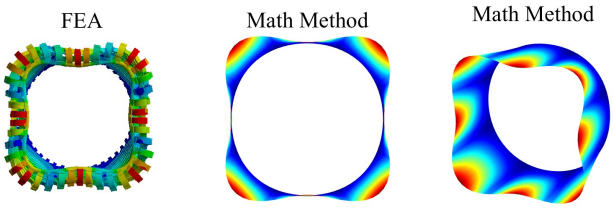


Fig11. Four-lobed.

It can be seen from the frequency distribution table that the natural frequencies comply with [17]. The frequency range of the ellipse shape natural frequency of the entire end should be avoided by "≤95Hz, ≥110Hz ". Furthermore, the data used

in the model refer to the data of a turbogenerator within a reasonable range and the results obtained from relevant literature. Thus, the model is correct and effective, and the modal analysis is also of the reference value.

The comparison between Table IV and Figs. 8-11 highlights the alignment between the two vibration patterns, with the maximum error in modal frequency not exceeding 9%. The findings confirm the accuracy of the proposed equivalent model.

The mathematical model established in this paper serves as the basis for this investigation. Based on the mathematical model, the present study investigates the influence of the physical parameters of the wire rod, a key component of the structure, on the modal frequency of the structure.

Fig. 12 illustrates the variation in modal frequencies for different orders when Young's modulus of the wire rod is increased to 1.2$E$. The horizontal coordinates represent the modal orders, corresponding to order 1 to shake type, order 2 to Ellipse type, order 3 to Three-lobed, and order 4 to Four-lobed. The vertical coordinates represent the change in modal frequency with the relative rate of change. The relative rate of change is positive for each order, indicating that the modal frequency increases with an increase in Young's modulus in each order. The rate of change is most significant in order three and lowest in order 1. The variation in inherent frequency increases with the order number. The structure's overall stiffness increases when Young's modulus of the wire rod increases, and therefore the inherent frequencies of each order increase.

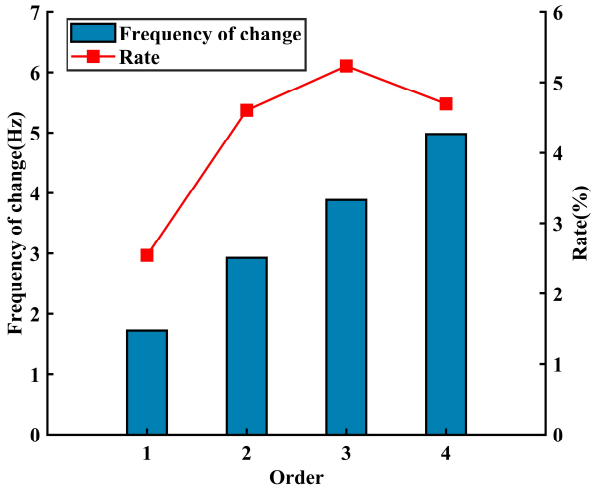


Fig12. Effect of Young's modulus $E$ on modal frequency.

Fig. 13 illustrates the variations in the modal frequencies for each order as the wire rod density $\rho$ is increased to 1.2$\rho$. The horizontal coordinates represent the modal orders, while the vertical coordinates represent the change in modal frequency as a relative rate of change. The relative rate of change for each order is close to -8.672%, indicating that the modal frequency decreases with the increase of the wire rod density. The influence of the wire rod density on each order is nearly the same. It can be inferred that the negative correlation between the intrinsic frequency and the density is consistent for each structure order. As the wire rod's density increases, the structure's overall mass increases, resulting in the decrease of the order frequencies.

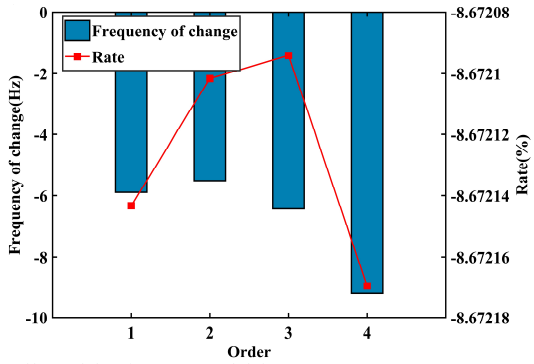


Fig13. Effect of density $\rho$ on modal frequency.

Fig. 14 presents the variation of the modal frequencies for different orders with a change in Poisson's ratio $\mu$ to 1.2$\mu$. The relative rate of change observed is positive and is within 1%, indicating that an increase in Poisson's ratio increases the inherent frequency of each structure order. The effect of Poisson's ratio on the inherent frequency of each structure order is found to be low.

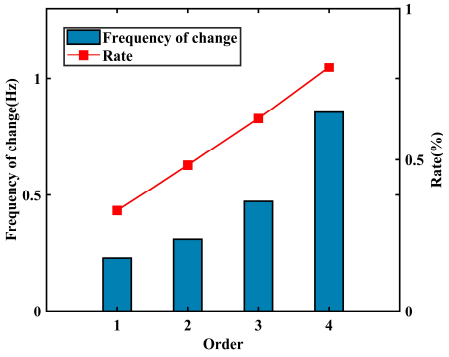


Fig14. Effect of Poisson's ratio $\mu$ on modal frequency.

The influence of individual physical parameters of the wire rod on the modal frequencies of each structure order is illustrated in Figs. 15-17. Fig. 15 demonstrates the positive correlation between each structure order's inherent frequency and Young's wire rod modulus, with a lower slope of the curve observed for the mode shake type than the other three modes. Fig. 16 depicts the negative correlation between the intrinsic frequency of each structure order and the density of the wire rod, with a nearly uniform slope of the curve for each mode order. Fig. 17 highlights the positive correlation between each structure order's inherent frequency and Poisson's ratio of the wire rod. However, the correlation is weak, indicating a limited effect of Poisson's ratio on the inherent frequency of the structure.

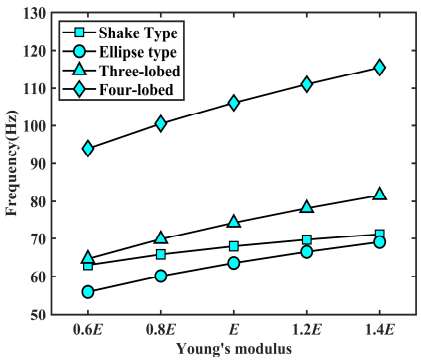


Fig15. Influence of Young's modulus $E$ on modal.

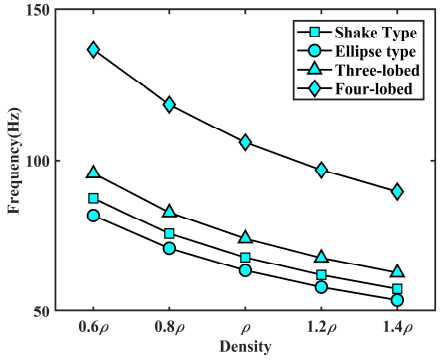


Fig16. Influence of density $\rho$ on modal.

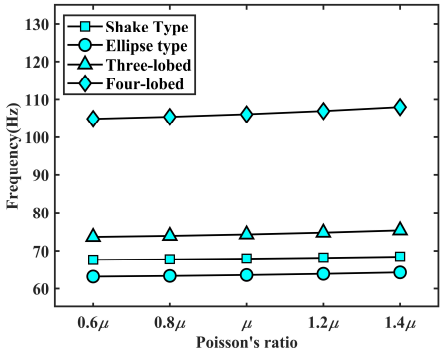


Fig17. Influence of Poisson's ratio $\mu$ on modal.

Based on Figs. 12-17, the primary physical parameters influencing the modal frequency of the structure are Young's modulus and the density of the wire rod. The correlation between Young's modulus and the modal frequency is positive. However, it differs for each order of frequency. It is demonstrated that the overall mass and stiffness of a structure is affected by adjusting the Young's modulus and density, which adjusts the inherent frequency of the structure accordingly. This conclusion provides valuable insight for optimizing the stator end winding structure.

The physical properties of the wire rod, specifically Young's modulus and density, were deemed to be the most crucial factors affecting the inherent frequency of the winding equivalent structure. In order to assess the effect of these properties on the intrinsic frequency, a bivariate experiment was designed. The change in frequency at each order was investigated in this study by modifying the values of Young's modulus and density, as shown in Figs. 18-21.

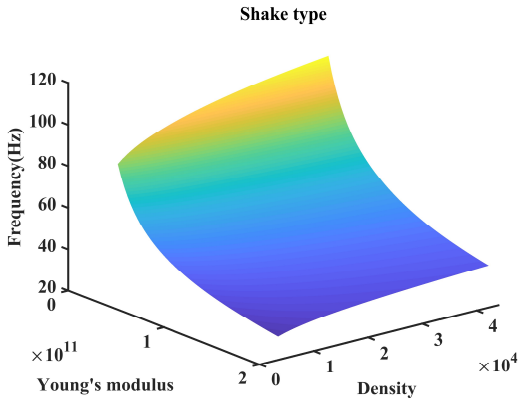


Fig18. The effect of $E$ and $\rho$ on the frequency of the shake type of structure.

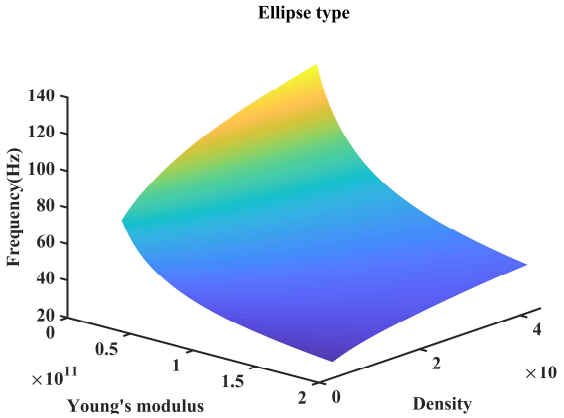


Fig19. The effect of $E$ and $\rho$ on the frequency of the ellipse type of structure.

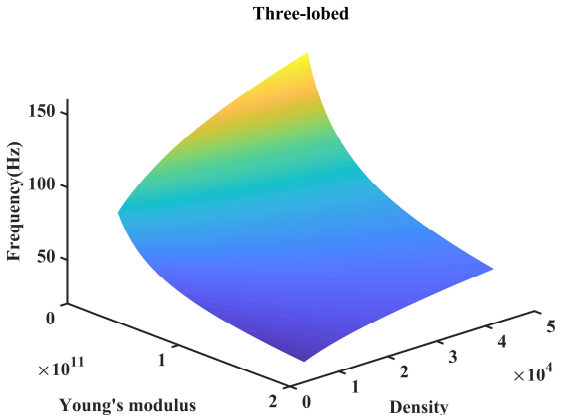


Fig20. The effect of $E$ and $\rho$ on the frequency of the three-lobed of structure.

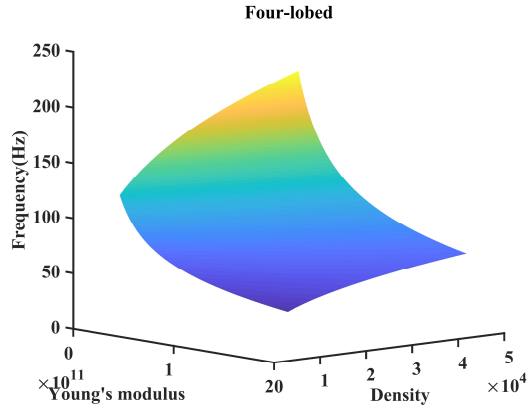


Fig21. The effect of $E$ and $\rho$ on the frequency of the four-lobed of structure.

Figs. 18-21 depicts the relationship between the frequency of each vibration order and the material's physical properties. The graph reveals a decline in frequency as Young's modulus increases and density decreases. The consistency in the surface type for each order of vibration suggests that the intrinsic frequency of the material exhibits a similar pattern of variation with changes in both Young's modulus and density. Further analysis of the curvature of the surfaces indicates that the influence of Young's modulus on intrinsic frequency is more pronounced than the effect of density.

## IV. Conclusion

The complexity of the end winding poses a challenge for its full consideration in the finite element model and digital model. An equivalent model of the wire bar based on a three-point bending test was employed to address this issue. Young's modulus and density of the equivalent wire rod can

be obtained by keeping the wire's mass, section length, and section width of the wire. Thus, the equivalence model of the wire bar can be obtained.

We then applied the equivalent wire rod to develop a digital mechanism model. This study simplified the helical structure to a composite shell structure, and its characteristic vibration equations are established using the energy method. A comparison with the finite element analysis shows the correctness of the digital mechanism model. The influence of the material parameters of the main components on the modal frequencies was investigated through mathematical modeling, revealing that Young's modulus and the wire rod density had positive and negative correlations with the inherent frequencies at each order, respectively. On the other hand, Poisson's ratio was found to have a weak impact on the inherent frequencies.

This study's results can aid in optimizing the stator end winding structure of the turbine generator. The equivalence model proposed in this paper can also assist in digital modeling for big data applications.

## REFERENCES


[1] Yuan Changjian, Yi Ran, Lan Bo. “Analysis of the structure of the stator end of a large turbogenerator,” Technology of Large Electric Machines, vol. 8, pp. 91-94, 2005.

[2] Zhou Y , Zhang Q L, Duan J G. “Dynamical characteristics and influencing factors of stator end-windings of a turbine generator analyzed via heterogeneous element fusion modeling,” Energy Reports, vol. 7, pp. 658-672, 2021.

[3] S. Lange and M. Pfost, “Analysis of the Thermal Influence on the Vibrational Behavior of the Stator End-Winding Region, ” 2019 International Aegean Conference on Electrical Machines and Power Electronics (ACEMP) & 2019 International Conference on Optimization of Electrical and Electronic Equipment (OPTIM), pp. 108-113, 2019.

[4] Ruan Jiangjun, Chen Xianzhen, Zhou Keding. “Three-dimensional analytical representation of the involute of the stator coil end in the calculation of the 3D eddy current field at the end of the turbogenerator,” Large Electric Machine Technology, vol. 6, pp. 21-24, 1995.

[5] H. Jichao, W. Chao, W. Yang, et al. “Influence of Extension Length of Rotor End Windings on the Three-Dimensional Electromagnetic Field and Temperature Rise in the Large Turbine Generator End Zone With Magnetic Screen,” IEEE Access, vol. 8, pp. 70703-70712, 2020.

[6] Zhao Yang. “Investigation on the Structural Optimization Schemes of Large Turbogenerator Stator End Winding,” Chongqing University, 2015.

[7] Wang Xiaofang. “Research on Parametric Modeling Method of Hydrogenerator Stator Bar Based on NX,” Large Electric Machine Technology, vol. 1, pp. 24-28, 2017.

[8] S. Lange and M. Pfost, “Analysis of Damping Models in a Structural Mechanical 3D-FE Stator End-Winding Region Model,” 2018 XIII International Conference on Electrical Machines (ICEM), pp. 52-57, 2018.

[9] P. G. S. Kumar, K. M. Reddy and K. K. Kumar, “Reinforcement of Generator Stator End Winding Structure by Modal Analysis Approach, ” 2019 IEEE 4th International Conference on Condition Assessment Techniques in Electrical Systems (CATCON), pp. 1-5, 2019.

[10] Jones, R.M. Mechanics of Composite Materials. Boca Raton: CRC Press, 1999.

[11] Oya A, Navarro-Moreno J, Ruiz-Molina J C, et al. “A Numerical Technique for Simulating Linear Operations on Random Fields,” IAENG International Journal of Applied Mathematics, vol. 37, no. 2, pp. 107-111, 2007.

[12] Johri T, Johri Im, “Study of Exponential Thermal Effect on Vibration of Non-Homogeneous Orthotropic Rectangular Plate Having Bi-Directional Linear Variation in Thickness,” Lecture Notes in Engineering & Computer Science, vol. 1, 2011.

[13] Leissa A W. Vibration of shells. New York: Acoustical Society of America, 1993.

[14] Tian L, Ye T, Jin G. “Vibration analysis of combined conical-cylindrical shells based on the dynamic stiffness method,” Thin-Walled Structures, vol. 159, no. 4, pp. 107260, 2020.

[15] Li W L. “Vibration analysis of rectangular plates with general elastic boundary supports,” Journal of Sound and Vibration, vol. 273, no. 3, pp. 619-635, 2004.

[16] Civalek O. “Numerical analysis of free vibrations of laminated composite conical and cylindrical shells: Discrete singular convolution (DSC) approach,” Journal of Computational & Applied Mathematics, vol. 205, no. 1, pp. 251-271, 2007.

[17] People's Republic of China Electric Power Industry Standard. Measurement and Evaluation of Dynamic Characteristics of Large Wind Turbine Generator Stator Windings End.